Statistical Dependence of Albedo and Cloud Cover on Sea Surface Temperature for Two Tropical Marine Stratocumulus Regions

LAZAROS OREOPOULOS AND ROGER DAVIES

Department of Atmospheric and Oceanic Sciences, McGill University, Montreal, Quebec, Canada

(Manuscript received 14 January 1993, in final form 13 May 1993)

ABSTRACT

The relationship between sea surface temperature (SST) and albedo or cloud cover is examined for two tropical regions with high values of cloud radiative forcing and persistent marine stratocumulus (mSc)—one off the west coast of Peru, the other off the west coast of Angola. The data span five years, from December 1984 to November 1989. Albedos are from the Earth Radiation Budget Experiment, cloud covers are from the International Satellite Cloud Climatology Project, and SSTs are from the Climate Analysis Center.

Negative correlation coefficients between albedo and SST are found to be about −0.8 when the seasonal variation of the entire dataset is analyzed. The interannual variation and the spatial variation of individual months also yields correlation coefficients that are negative. The correlation between cloud cover and SST is found to be similar to but weaker than the correlation between albedo and SST, suggesting a decrease in cloud amount and a decrease in cloud albedo with increasing SST for these regions. The corresponding albedo sensitivity averages $-0.018\ K^{-1}$ with local values reaching $-0.04\ K^{-1}$. These findings are valid from 19°C to 25°C for the Peru mSc and 22°C to 27°C for the Angola mSc. These temperatures approximately bound the domains over which mSc is the prevalent cloud type within each region.

These results imply a potential positive feedback to global warming by marine stratocumulus that ranges from $\sim 0.14\ W\ m^{-2}\ K^{-1}$ to $\sim 1\ W\ m^{-2}\ K^{-1}$, depending on whether or not our results apply to all marine stratocumulus. While these values are uncertain to at least ±50%, the sensitivity of albedo to sea surface temperature in the present climate may serve as a useful diagnostic tool in monitoring the performance of global climate models.

1. Introduction

The importance of clouds in the earth's climate system is well recognized, especially their role in reflecting solar radiation, and in absorbing and emitting longwave radiation. Their net effect on radiation at the top of the atmosphere may be evaluated using the concept of cloud radiative forcing, defined as the difference in net radiative flux between average and clear-sky conditions (Ramanathan et al. 1989). This forcing varies with cloud type, from weak positive forcing characteristic of cirrus to strong negative cloud radiative forcing characteristic of marine stratocumulus (mSc). Local seasonally averaged values of net forcing in regions covered by mSc can be as high as $-80\ W\ m^{-2}$ in the tropics (Oreopoulos 1992) and over $-100\ W\ m^{-2}$ in higher latitudes (Harrison et al. 1990), depending on the season. On a global scale, cloud radiative forcing is negative, as shown by measurements from the *Nimbus-7* satellite and the satellites of the Earth Radiation Budget Experiment (ERBE) (Ramanathan et al. 1989; Harrison et al. 1990; Stephens and Greenwald 1991; Ardanuy et al. 1991).

The potential for cloud radiative feedback in climate change is also well recognized, but many questions remain to be answered, especially on how the climate system affects cloud properties, including their formation and dissipation. It is, for example, very difficult to predict the response of cloud distribution and microphysical properties to climate forcing. General circulation models (GCMs) can be used for this purpose but their present treatment of clouds limits the confidence of their predictions (Cess et al. 1990). There is clearly a need for improved theories of cloud formation, evolution, and dissipation as well as for semiempirical relationships between cloud properties and climate variables. This is particularly true for boundary-layer clouds such as mSc, which are poorly represented in GCMs (Cess et al. 1990; McFarlane et al. 1992).

High pressures, subsidence, and cold oceans characterize the regions of mSc (Newell et al. 1974). Low-level mixing takes place within the cloud-topped boundary layer, and the vertical development of mSc is inhibited by the trade-wind inversion (Riehl 1979). The suggestion (Lilly 1968) that turbulent energy generation by infrared cloud-top cooling drives the boundary-layer dynamics and sustains the clouds has

Corresponding author address: Lazaros Oreopoulos, Dept. of Atmospheric and Oceanic Sciences, McGill University, 805 Sherbrooke St., W., Montreal, Quebec H3A 2K6, Canada.

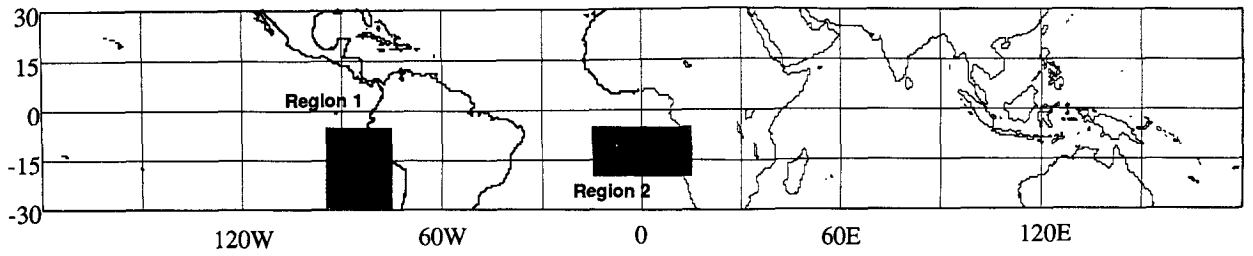

FIG. 1. The two mSc-dominated regions selected to examine the relationship between SST and albedo/cloud cover.

stimulated a great amount of modeling (Schubert 1976; Kahn and Businger 1979; Schubert et al. 1979; Deardorff 1980a; Moeng and Arakawa 1980; Chen and Cotton 1983; Bougeault 1985; Turton and Nicholls 1987; Duynkerke and Driedonks 1987). To further improve understanding of the processes affecting mSc behavior, a multidisciplinary field experiment called the First International Satellite Cloud Climatology Project (ISCCP) Regional Experiment (FIRE) took place off the west coast of California in 1987 (Randall et al. 1984; Albrecht et al. 1988). Results from FIRE have been presented by, amongst others, Fairall et al. (1990), Albrecht et al. (1990), Betts (1990), Paluch and Lenschow (1991), Blaskovic et al. (1991), and Nucciarone and Young (1991). Cloud breakup or dissipation mechanisms that have drawn much attention are cloud-top entrainment instability (CTEI) [various criteria have been developed for its initiation, see Randall (1980), Deardorff (1980b), Kuo and Schubert (1988), MacVean and Mason (1990), Albrecht (1991)] and the cloud–subcloud-layer decoupling first described by Nicholls (1984).

The global importance of large-scale mSc variability has not attracted much attention until recently. Hanson (1991) used a 40-year climatology of cloud cover and SST in a study of the interannual variability of three mSc regimes. This study demonstrated the existence of a weak contemporaneous correlation between these variables, with warmer months tending to be less overcast on average. Peterson et al. (1992) performed an interannual analysis of SST anomalies and cloud anomalies derived from *Nimbus-7* observations, and also found that increases in cloud cover are associated with decreases in SST. Finally, Klein and Hartmann (1993) used climatological cloud cover and a measure of static stability (the potential temperature difference between 700 mb and the surface) to demonstrate that a strong positive correlation exists between these two variables for tropical and subtropical mSc.

The potential of mSc for an important cloud radiative feedback arising from their strong radiative forcing, their poor representation in GCMs, and the need to extend the current knowledge on the large-scale variability of these clouds provides motivation for the present paper. Using five years of ERBE data, we address the apparent dependence of albedo on sea surface temperature (SST) from a seasonal, spatial, and interannual perspective. SST and cloud amount relationships are examined as well. The dataset used and the regions selected for analysis are discussed in the next section. Section 3 examines the correlation between SST and albedo on an annual, interannual, and spatial basis, including its dependence on SST and the extent to which albedo and cloud cover can be used interchangeably. The sensitivity of albedo to SST is discussed in section 4 followed by a section on the climatic implications of our analysis.

2. Data sources

Five full years (December 1984–November 1989) of albedo (a), total cloud cover (TCC), and SST for two rectangular tropical oceanic regions that tend to be dominated by mSc clouds were analyzed. As shown in Fig. 1, Region 1, off the west coast of Peru, is bounded in latitude by 5°S and 30°S, and in longitude by 95°W and 75°W, and Region 2, off the west coast of Angola, is between 5°S and 20°S, and between 15°W and 15°E.

While these are primarily oceanic regions, the desire to include coastal ocean caused some land to be included as well. Region 1 consists of 80 2.5° × 2.5° grid cells, 6 of which contain land. Eight of the 72 grid cells that make up Region 2 contain land. However, values that correspond to land grid points have been excluded from the subsequent analysis. These regions were chosen primarily because they exhibit minimal longwave flux variability throughout the year, indicating negligible influence from tropical convection and extratropical weather systems. Another factor that simplifies their study is the relatively low seasonal variation of solar zenith angle. Despite remaining equatorward of the subtropical high pressure centers, both regions nonetheless exhibit high annual variability in albedo and cloud cover.

The mSc region off the coast of California is also known to be persistent, but appears to be more complicated to study due to its more subtropical nature. It exhibits significant annual variability in its longwave emission (Oreopoulos 1992) and has somewhat greater amounts of nonstratiform clouds (Warren et al. 1988), suggesting a greater level of baroclinic activity. It also

extends poleward of the subtropical high to ~40°N, causing a greater seasonal range of albedo due to changing solar declination. The added complexity of this region made a simple search for correlations rather pointless and it was not included in our study.

The albedo data were monthly means at a spatial resolution of 2.5° × 2.5° obtained from the Earth Radiation Budget Experiment (Barkstrom et al. 1989), and more specifically from the scanner of the ERBS satellite. The albedos from this satellite alone were selected to obtain the longest self-consistent time series. Total cloud cover was from ISCCP (Rossow and Schiffer 1991). It is retrieved from visible and thermal infrared radiances collected from various polar orbiting (NOAA) and geostationary (GOES, GMS, METEOSAT) satellites and is also available on a 2.5° × 2.5° grid. Ocean surface temperatures were from the blended (in situ–AVHRR satellite) Climate Analysis Center (CAC) SST analysis. A complete description of the analysis procedures is given by Reynolds (1988). The SST fields are monthly and available on a 2° × 2° grid. To compare the SST fields with the fields of albedo and cloud cover, they were first degraded to 2.5° × 2.5° resolution by linear interpolation.

3. Correlations between sea surface temperature and albedo

a. Annual variability

Figure 2 displays the annual cycle of SST and albedo for Regions 1 and 2. These are 5-yr averages over the entire domain of each region excluding land. The SST cycle in both regions is a smooth, almost sinusoidal, variation over the year, with an amplitude of about 2.5 K, maximum in March and minimum in September. Both regions behave similarly, although Region 2, extending only to 20° S, is substantially warmer than Region 1. The albedo cycles, although less smooth, are nonetheless almost completely out of phase with the SSTs. Maximum albedo occurs in September (both regions), and minimum albedo in February (Region 2) or March (Region 1).

The relationship between SST and albedo suggested by Fig. 2 is in agreement with other data for the same regions, notably climatological SST (Bottomley et al. 1990; Mitchell and Wallace 1992) and cloud cover (Warren et al. 1988), the June 1974–February 1978 albedo from NOAA and *Tiros-N* satellites (Mitchell and Wallace 1992), and the ISCCP cloud cover for the same 5-yr period (our analysis, not shown). Such a striking relationship is consistent with the sea surface temperature directly affecting the albedo in regions covered by this cloud type. Owing to their large thermal inertia, oceans respond to seasonal changes in insolation with a 2-month delay (Riehl 1979), so that the reverse effect, that of cloud cover affecting sea surface temperature, is unlikely. The relationship is also consistent, however, with the possibility that both SST and albedo are simply responding to the annual cycle of some other meteorological variable.

A time-lag analysis using the monthly mean values of albedo and SST showed a maximum (negative) correlation for zero lag in Region 2, and when SST lagged albedo by 1 month in Region 1. While we cannot dismiss the latter correlation as insignificant, we believe that it is the contemporaneous correlation that most likely expresses the physics of sea–cloud interactions in these regions. To support this view we note that the time series is too short for a more robust analysis and the −1 lag may arise as an artifact; contemporaneous correlations for Region 1 are better than −1 lag correlations in the other types of variability discussed later; time-lag analysis with spatially averaged SST and ISCCP TCC give the same value of correlation coefficients for 0 and −1 lag; Hanson (1991) found his best

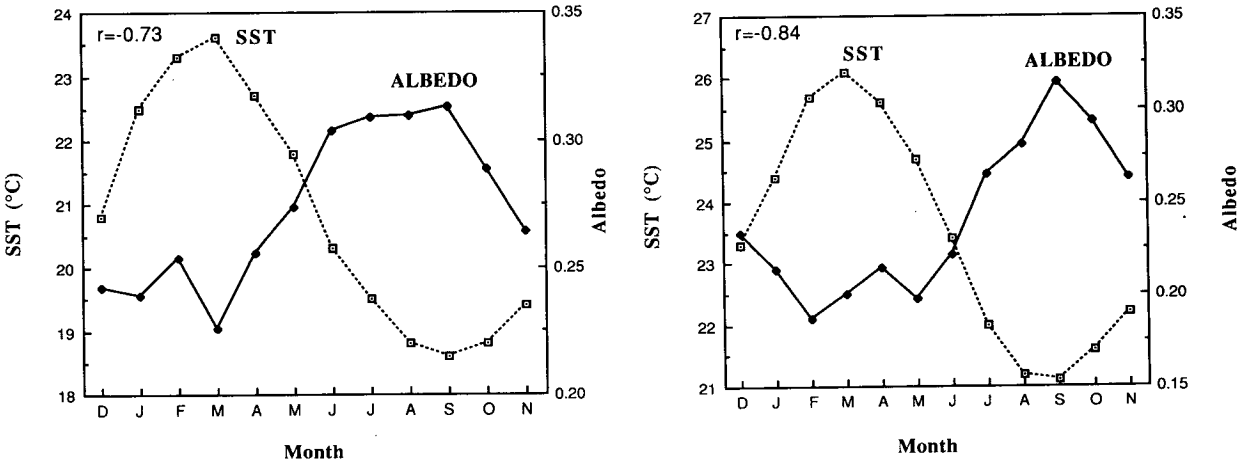

FIG. 2. Annual cycle of spatially averaged SST (dashed) and albedo (solid) and coefficient of linear regression from 60 monthly averages (Dec84–Nov89) for Region 1 (left) and Region 2 (right).

SST–cloud amount correlations at 0 lag; and 1 month seems too small a time lag for SSTs of the open ocean to respond to changes in solar forcing—2 months agrees more with meteorological experience (Riehl 1979). However, we also note that Mitchell and Wallace (1992) imply that both correlations may be important; they discuss the existence of a positive feedback loop where more clouds cause lower SSTs, which in turn (via an unknown mechanism) cause more clouds. Here we argue that it is the ocean circulation (upwelling) that mainly drives the SST. Finally, note that the +1 lag correlation (SST leading clouds) is poor for all the types of variability we examined, a result consistent with our knowledge of the time scales of atmospheric response to external forcing.

The correlation coefficients of linear regression between SST and albedo at zero lag from the 60 monthly averages are −0.73 for Region 1 and −0.84 for Region 2. Both coefficients are statistically significant at the 99% level even if only 25% of the data are considered independent.

It would be interesting to know how SST and albedo are correlated, not only in the domain average but also within each domain. Correlation coefficients were therefore calculated for each grid point from the 60 monthly mean values and the fields obtained are shown in Fig. 3. Region 2 has a considerably more homogeneous correlation field than Region 1. The packing of the contours at the right edges of both regions is due to the transition to land where the correlations break down. There is a clear tendency in Region 1 for the correlations to be strongest near the coast. If these fields are compared with the 5-yr average fields of albedo and SST (Fig. 4), a tendency for the correlations to deteriorate at the vicinities of extreme (either "cold" or "warm") SST is observed. Moreover, the regions of best correlation do not coincide with the regions of annual albedo maxima. The SST–TCC correlation coefficient fields (not shown) are similar.

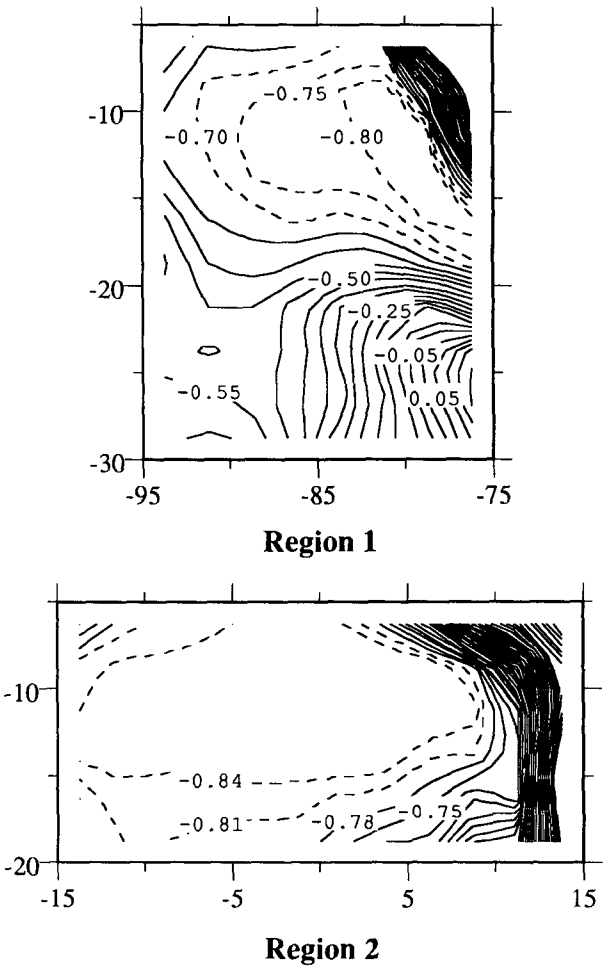

FIG. 3. Fields of correlation coefficients derived from annual variability. The contour interval is 0.05 in Region 1 and 0.03 in Region 2. The local maxima are highlighted by the dashed contours. The packing of contours at the right edges is due to the transition to land.

b. *Interannual variability*

The current dataset spans only 5 years and is too short for the comprehensive analysis of interannual variability. However, it can be used in a simple manner to test the hypothesis that albedo and SST remain anticorrelated under interannual variation.

The method used was that for each month and for each grid point, 5-yr averages were calculated and 60 anomaly fields for each region were created by subtracting the average values from the monthly values for each variable. Thus

$$\Delta a_{i,j} = a_{i,j} - a_{i,k} \quad (1a)$$

and

$$\Delta \mathrm{SST}_{i,j} = \mathrm{SST}_{i,j} - \mathrm{SST}_{i,k} \quad (1b)$$

where $\Delta a_{i,j}$ and $\Delta \mathrm{SST}_{i,j}$ are the albedo and SST anomalies for the ith grid point of the jth month; $a_{i,j}$ and $\mathrm{SST}_{i,j}$ are the individual monthly values; and $a_{i,k}$, $\mathrm{SST}_{i,k}$ are the 5-yr averages for the kth month. That is, j equals k or differs by a multiple of 12. From the 60 × 74 anomaly pairs of Region 1, only those with $|\Delta a_{i,j}| > 0.05$ and $|\Delta \mathrm{SST}_{i,j}| > 0.5$°C were selected. From the 60 × 64 anomaly pairs of Region 2, only those that have both $|\Delta a_{i,j}| > 0.025$ and $|\Delta \mathrm{SST}_{i,j}| > 0.5$°C were selected. These thresholds were chosen somewhat arbitrarily as a compromise between eliminating the noise of measurement error or natural variability and ensuring that a sufficient number of points were left to reach statistical conclusions. Consequently, the SST anomaly threshold is lower than the estimated rms error in the SST monthly values [±0.8 K, see Reynolds (1988)], and the albedo anomaly threshold is higher than the estimated uncertainty of ±0.014 (Harrison et al. 1990). The albedo threshold for Region 2 was set

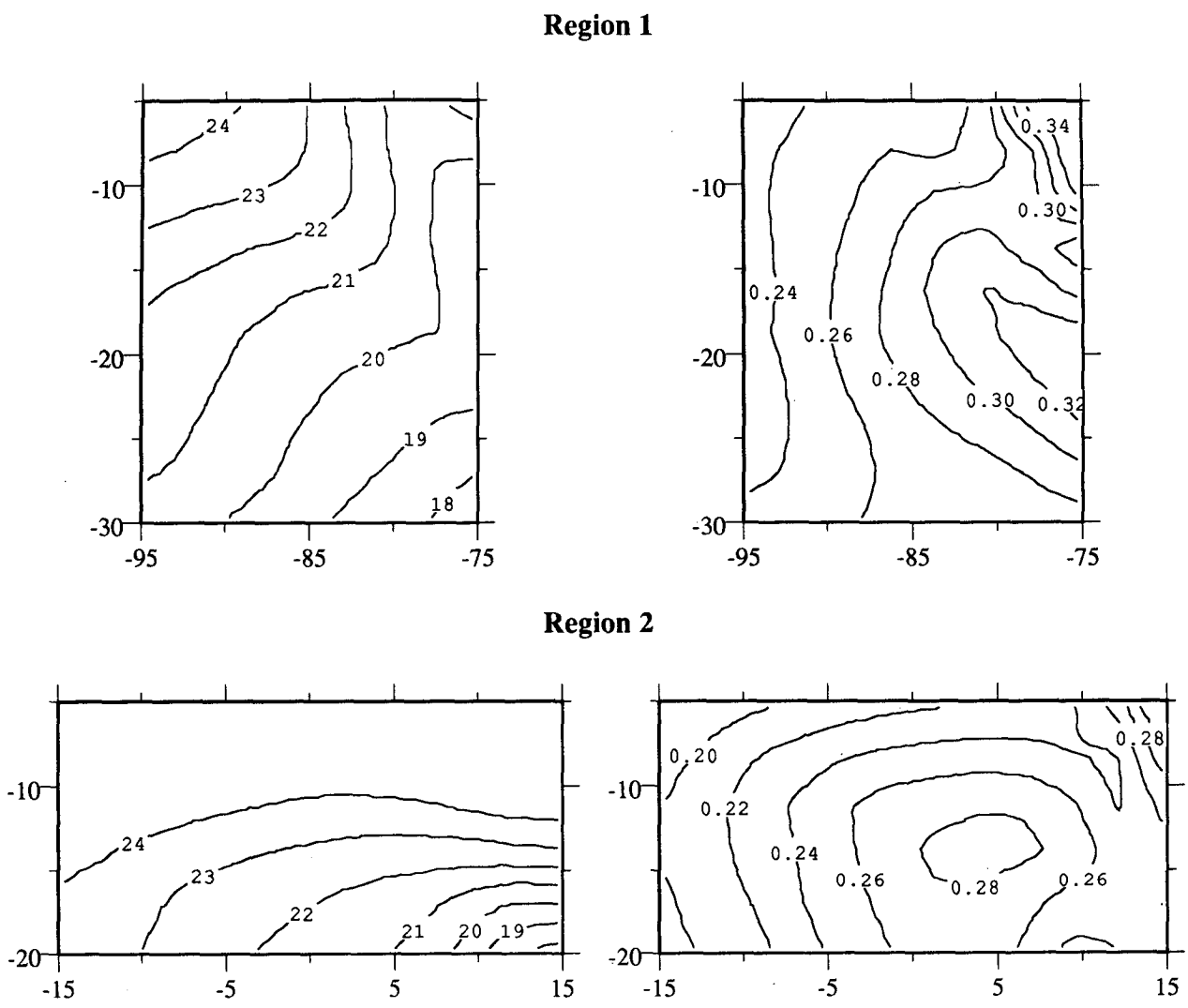

FIG. 4. Sixty-month average fields of SST (left) and albedo (right) for both regions.

lower than for Region 1 because less interannual variability in albedo is observed for that region. By setting such thresholds, the remaining points are more likely to be associated with real cloud responses to anomalous cooling or warming events.

All pairs of SST and albedo satisfying the above criteria were plotted on the SST–albedo plane and appear as the scatter diagrams shown in Fig. 5. Each plot has been divided into four quadrants. The number of points lying on each quadrant is also shown. Over 90% of the points fall somewhat evenly in the first and third quadrants of both regions. These results indicate that interannual variations of SST and albedo occur in such a way that unusual cooling (warming) of a particular pixel tends to be associated with increased (decreased) albedo. This is in excellent qualitative agreement with the results from annual variability.

The statistical significance of the results in Fig. 5 may be limited by the fact that many points in the first and third quadrant originate from relatively few months. More specifically, 50% of the points in Region 1 come from four months (Jan 1985, Nov 1986, Oct 1988, and Oct 1989) while 39 months contribute no anomalies. In Region 2, 33% of the points come from four months (Jan 1986, Jul 1987, Nov 1987, and Mar 1988) while 25 months contribute no anomalies. Hence, some of the anomaly pairs may be spatially autocorrelated and not independent. It seems clear, however, that the dominance of negative correlations between albedo and SST is not a coincidental result due to the subjective elimination of data or the influence of isolated synoptic events. When the albedo filter is "turned off," 63% of the points in Region 1 and 73% of the points in Region 2 still lie in the anticorrelation quadrants. A similar analysis using SST and ISCCP cloud cover gave similar results—85% and 90% of the points were in the anticorrelation quadrants for Regions 1 and 2, respectively, consistent with the inter-

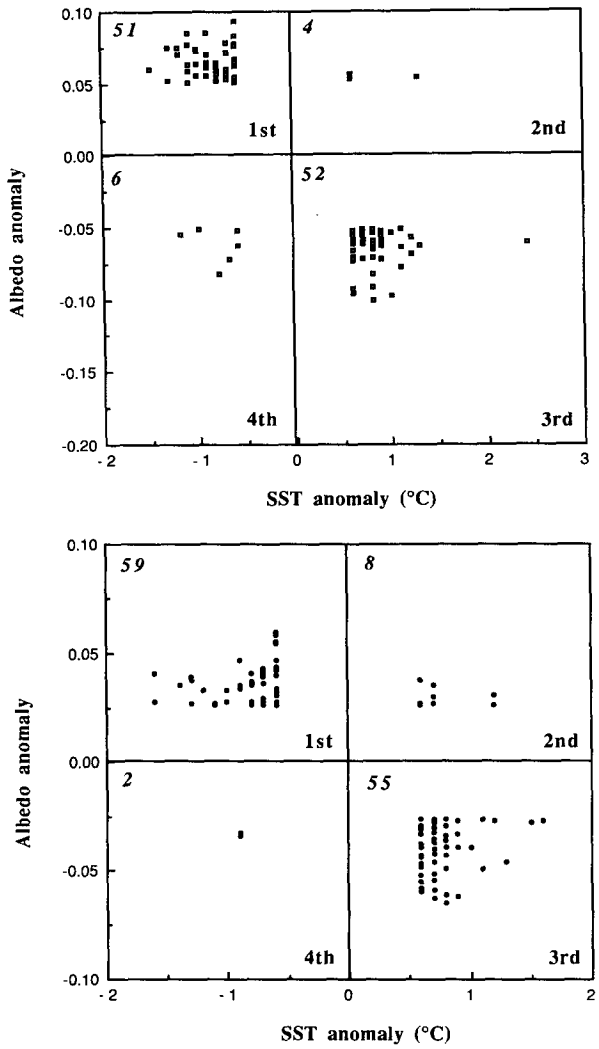

FIG. 5. Grid points with $|\Delta a| > 0.05$ and $|\Delta \mathrm{SST}| > 0.5°\mathrm{C}$ (Region 1, top) and $|\Delta a| > 0.025$ (Region 2, bottom). The number of points in each quadrant is given.

annual results of Hanson (1991), Peterson et al. (1992), and Klein and Hartmann (1993; their Fig. 16).

c. Spatial variability

We also examined the spatial variability within each region to determine whether for each individual month the colder grid points have higher albedos. This time we calculated anomalies with respect to the domain average for each month. Correlation coefficients between SST and albedo were estimated for each region and for each month using the formula

$$r_k = \frac{\sum_{i=1}^{N} (\mathrm{SST}_{i,k} - [\mathrm{SST}]_k)(a_{i,k} - [a]_k)}{\left\{ \sum_{i=1}^{N} (\mathrm{SST}_{i,k} - [\mathrm{SST}]_k)^2 \sum_{i=1}^{N} (a_{i,k} - [a]_k)^2 \right\}^{1/2}} \quad (2)$$

where $\mathrm{SST}_{i,k}$ and $a_{i,k}$ are the SST and albedo of the ith grid point in the kth month, $[\mathrm{SST}]_k$ and $[a]_k$ are the spatial averages for the kth month, and N is the number of grid points (74 for Region 1 and 64 for Region 2).

The time series of the correlation coefficients for each month and for each region as calculated from Eq. (2) are shown in Fig. 6 (solid lines). The correlation coefficients have a wide range of values but most are negative. Only three months (Dec 1985, 1987, 1988) in Region 2 and four (Oct 1985, Nov 1986, Aug 1987, Aug 1989) in Region 1 have positive correlation coefficients. Unfortunately, there is no easy way to estimate accurate confidence limits for r_k because of the limited spatial resolution of the data and the fact that albedo and SST are spatially autocorrelated in a different way each month. While we have not determined the number of correlation coefficients that are statistically significant, we have estimated the mean correlation coefficient of the 60-month time series and its uncertainty. The means are -0.44 ± 0.09 for Region 1 and -0.39 ± 0.05 for Region 2, respectively. These results indicate that the anticorrelation between albedo and SST also exists spatially across Regions 1 and 2.

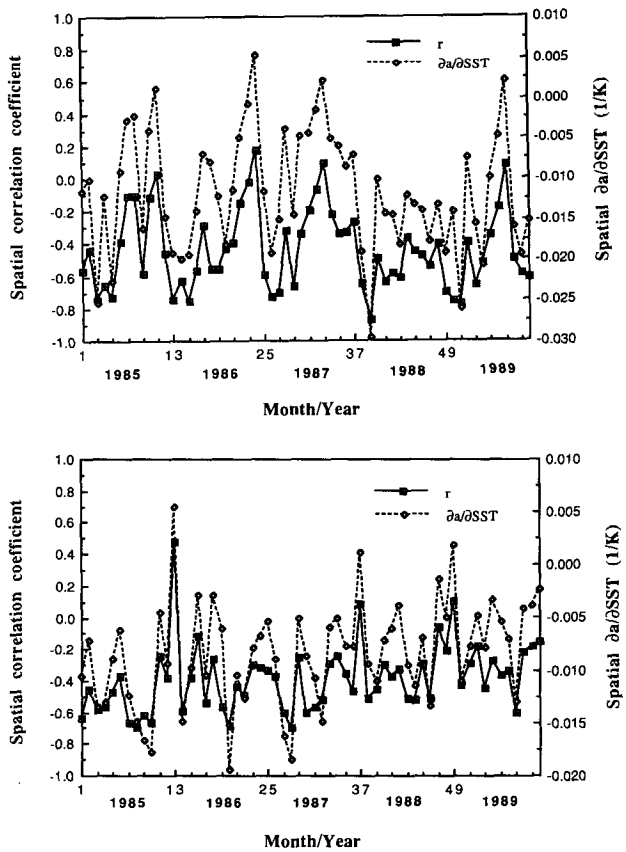

FIG. 6. Time series of correlation coefficient (solid line) and $\partial a/\partial \mathrm{SST}$ (dashed line) derived from spatial variability analysis for Region 1 (top) and Region 2 (bottom).

d. Correlation with cloud amount

We also examined the correlation of SST with total cloud cover and found generally similar results consistent with the dominant dependence of scene albedo on cloud amount. There were some differences, however, especially when the spatial variability of each region was considered on a monthly basis. More months with positive correlation were noted (35% for Region 1 and 10% for Region 2, including the same months that gave positive SST–albedo correlations) and the correlations were generally not as negative as with albedo.

Figure 7 compares the SST–albedo correlations with the SST–TCC correlations for both regions from the monthly analysis of spatial variability. Most of the points in Fig. 7 lie below the diagonal indicating a systematically better correlation between SST and albedo than between SST and TCC. This difference may not be surprising since total cloud cover and albedo are themselves not perfectly correlated—the albedo of an mSc pixel depends strongly on cloud optical thickness as well as cloud cover and can continue to change after the cloud cover saturates at 100%. It also appears that the retrieval of cloud cover may encounter difficulties at times, so that albedo is the more robust variable to use.

To illustrate the difficulty with retrieved cloud cover, Fig. 8 shows the fields of each variable for September 1988. This was a month when the correlation coefficients were very different (−0.48 for SST–albedo and 0.40 for SST–TCC). These fields indicate that while albedo drops with increasing SST in the direction of open ocean, the ISCCP cloud cover remains significant. The maxima of albedo and cloud cover also occur at different locations. In addition to the effect of cloud optical thickness, these differences could be associated with a number of difficulties in retrieving low-level cloud amount from bispectral thresholding. For example, as mSc breaks up, its albedo drops substantially, but the cloud amount can be overestimated by as much as 10% (Wielicki and Parker 1992) due to the partial field-of-view coverage problem. Some differences may also be due to the presence of cirrus, which can give relatively low albedos but have a strong enough longwave signal to be detected by the bispectral algorithm.

It is likely that patterns similar to those of Fig. 8 explain some of the differences between the SST–albedo and SST–TCC relationships. The systematically stronger correlation with albedo than with cloud cover, however, indicates that there may be some additional (negative) correlation of cloud albedo with SST for a fixed cloud amount. This does not appear to be consistent with the predictions of mixed-layer models (e.g., Schubert et al. 1979; Wang 1993) that suggest that cloud thickness increases along trajectories of increasing SST. It does, however, appear to be consistent with other observational evidence (Tseloudis et al. 1992) that indicates an apparent decrease of cloud optical thickness with increasing cloud temperature.

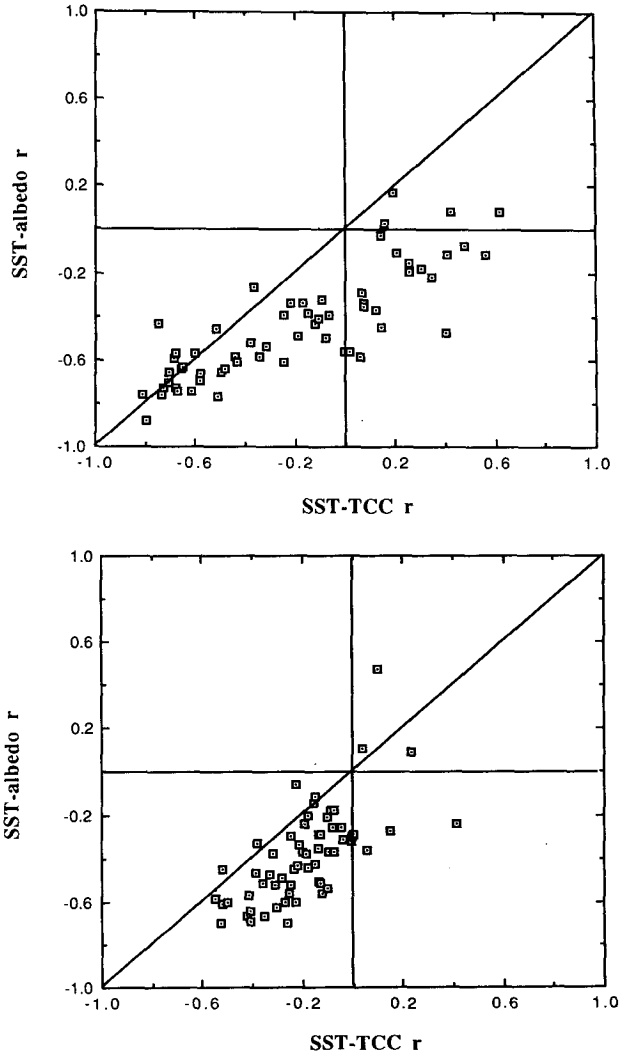

FIG. 7. Pairs of SST–albedo and SST–TCC spatial correlation coefficients for Region 1 (top) and Region 2 (bottom). The line of perfect fit is also shown.

e. SST dependence

The structure of the fields in Figs. 3, 4, and 8 implies that clouds diminish and correlations weaken at both the warm and cold limits of the SST range of the respective regions. In this section we accordingly examine the influence of temperature on the albedo–SST correlations.

Since the SST and albedo patterns show a seasonal north–south propagation, it is possible to examine seasonal changes of the correlation coefficients by evaluating them as a function of latitude within each region. This method also provides a consistency check for the spatial variability analysis of section 3c because it re-

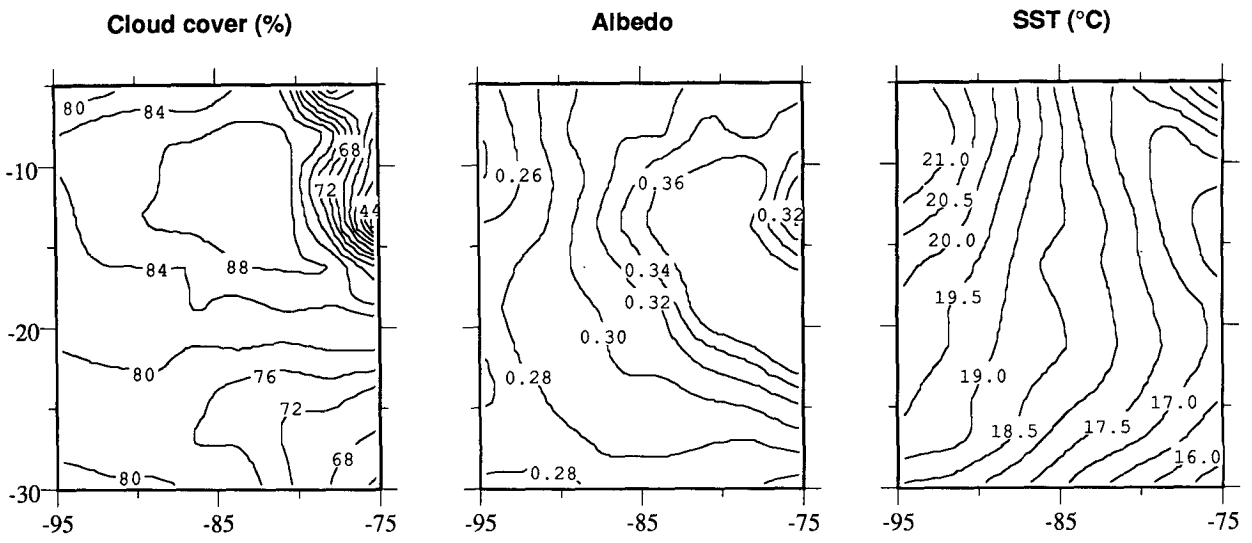

FIG. 8. Fields of SST, albedo, and TCC in region 1 for September 1988. Contour intervals are 0.5°C, 0.02, and 4%, respectively.

moves any dependence of the correlation on solar zenith angle. The main problem, however, with analyzing the data this way is that the correlation coefficients are estimated from very few pairs. Each latitude zone has about eight grid points in Region 1 (fewer in the latitudes where land grid points exist) and 11 grid points in Region 2. Fortunately, 60 months of data were available and this is sufficient to draw some conclusions.

Time–latitude cross sections of SST and the zonal correlation coefficient (after some smoothing to remove noise) are shown in Fig. 9. The cross sections of the correlation coefficients show coherent, almost periodic, patterns (especially in Region 2) with a good correspondence to the SST cross sections. Warm tongues of SST in Region 1 (above 25°–26°C) and in Region 2 (above 26°–27°C) in the northern half of the regions are generally associated with positive correlation coefficients, as are the coldest temperatures in Region 1 ($\leq$19°C). The unsmoothed correlation coefficient cross section for Region 2 also showed a tendency for positive values below 22°C but this feature does not appear in the smoothed field (except perhaps during months 42–44). Negative correlations occur mainly within the SST range that excludes these extreme values.

Another way to test the dependence of the correlation coefficients on SST is to stratify the spatial correlation coefficients in each month into different ranges of SST. Based on the behavior of the correlation coefficients in the previous analysis and after experimenting with various SST ranges, "cold," "intermediate," and "warm" ranges were chosen for each region. The divisions occurred at 19°C and 25°C for Region 1, and at 22°C and 27°C for Region 2. Correlation coefficients stratified by these temperature ranges were calculated for each month provided there were at least five data points available.

The results of this exercise are summarized in Table 1. The number of positive correlation coefficients exceeds that of negative coefficients in both "cold" and "warm" SST ranges for both regions. This result implies that the SST defines regimes where there is no longer the type of coupling with albedo demonstrated in our previous analysis. Note also that the "cold" and "warm" thresholds of Region 2 exceed those of Region 1 by approximately the amount by which Region 2 is warmer than Region 1.

In summary, there is evidence for a systematic change of the SST–albedo correlation with SST. This change refers to the sign reversal when "cold" ($\approx$19°C for Region 1, $\approx$22°C for Region 2) and warm ($\approx$25°C for Region 1, $\approx$27°C for Region 2) SST limits are crossed. These limits appear to mark the boundary of the marine stratocumulus, beyond which other cloud types with different responses to temperature may appear.

4. The sensitivity of albedo to changes in SST

The persistence of negative correlations, regardless of the way the SST–albedo coupling is examined, is a strong indication that, at least for the two regions examined here, there may be a direct sensitivity of mSc albedo to changes in sea surface temperature. It is therefore of interest to calculate this sensitivity, defined here as the partial derivative of albedo with respect to SST, and obtained by linear regression. In the case of annual variability, we can derive a single value of $\partial a/\partial$SST for each region if we use the spatial averages for each of the 60 months. We found $\partial a/\partial \text{SST} = -0.013$ K^{-1} for Region 1 and -0.022 K^{-1} for Region 2. These numbers are sensitive, however, to the way the domain is selected. If, for example, the domain had been restricted from the beginning so that it excluded many

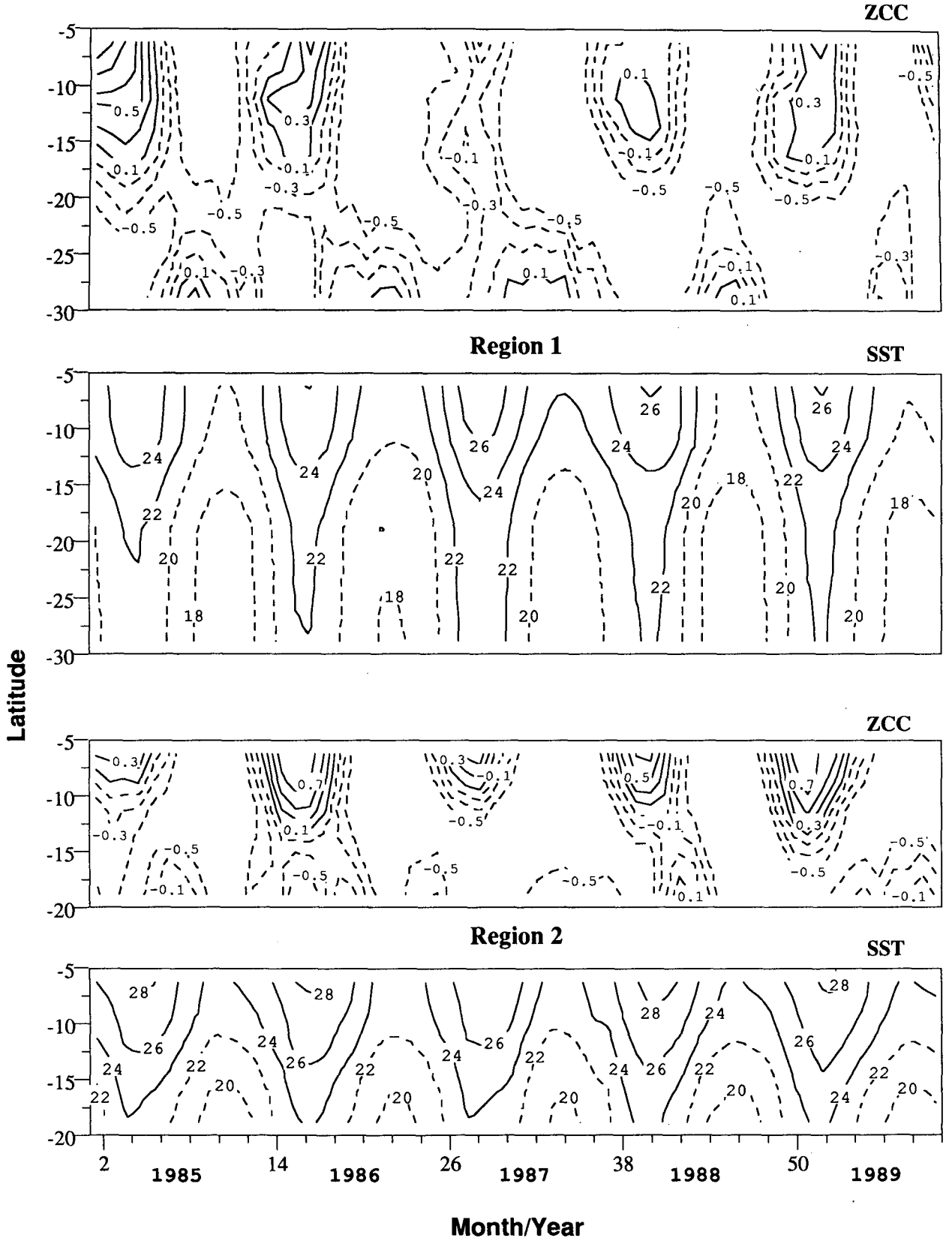

FIG. 9. Time–latitude cross sections of the zonal correlation coefficient (ZCC) and SST for Region 1 (upper panels) and Region 2 (lower panels). The ZCC patterns have been smoothed. Contour intervals are 0.2 for ZCC and 2°C for SST. The dashed contours are for ZCC ≤ 0, SST ≤ 20°C in Region 1 and SST ≤ 22°C in Region 2.

TABLE 1. Number of months with positive and negative spatial correlation coefficients for various SST ranges.

Region 1			Region 2		
SST category	$r \geq 0$	$r < 0$	SST category	$r \geq 0$	$r < 0$
≤19°C	21	14	≤22°C	27	13
19.1°–25°C	6	54	22.1°–27°C	3	57
>25°C	13	11	>27°C	14	6

of the grid points where the correlations deteriorate (see Fig. 3), the albedo sensitivity would have been more negative. If the weak correlations do indeed correspond to nonstratocumulus regimes, restricting the domain would yield a more accurate estimate of the mSc albedo sensitivity. This is illustrated in Fig. 10, which shows fields of $\partial a/\partial$SST constructed from the slopes of the regression line for albedo and SST for each grid point. As expected, the fields of $\partial a/\partial$SST are similar to the fields of correlation coefficients of Fig. 3. The maxima indicate that stronger albedo sensitivities, up to ≈ -0.04 K^{-1}, are possible locally.

When applied to cloud cover, the above analysis showed an average decrease of 3% K^{-1} in cloud amount for Region 1 and 6% K^{-1} for Region 2. This allows us to separate the total albedo sensitivity into that due to the change in cloud cover and that due to the change in cloud albedo. That is,

$$\frac{\partial a}{\partial \text{SST}} = \overline{\Delta a}\,\frac{\partial \text{TCC}}{\partial \text{SST}} + \overline{\text{TCC}}\,\frac{\partial a_{\text{mSc}}}{\partial \text{SST}} \qquad (3)$$

where $\overline{\Delta a}$ is the mean difference in albedo between cloud and clear sky, $\overline{\text{TCC}}$ is the mean cloud cover, and a_{mSc} is the albedo of a cloud pixel at the ISCCP resolution. We can assume the clear-sky albedo has no temperature dependence within these regions.

Taking as an example a nominal value of $\overline{\Delta a} = 0.25$, we find that the total albedo sensitivity of -0.013 K^{-1} for Region 1 may be subdivided into about -0.008 K^{-1} due to cloud cover changes and -0.005 K^{-1} due to local cloud albedo changes. Similarly, the total albedo sensitivity of Region 2 of -0.022 K^{-1} may be subdivided into -0.015 K^{-1} due to cloud cover changes and -0.007 K^{-1} due to local cloud albedo changes.

In principle, interannual variability can also be used to determine the albedo sensitivity. In practice, however, the linear regression depends on the subjective elimination of data. As the number of points used in the estimation of $\partial a/\partial$SST increases, more anomalies with values within the uncertainty range of the measurements enter the calculation. In addition, the scatter increases because of anomalies representing the natural variability of the system. It is thus hard to obtain an objective value of albedo sensitivity from interannual variability. Here we simply note that the albedo sensitivity corresponding to our original double threshold is ≈ -0.06 K^{-1} for Region 1 and ≈ -0.04 K^{-1} for Region 2. If we were to exclude data based on SST thresholding alone, these values would drop to -0.01 K^{-1} and -0.014 K^{-1}, respectively.

Figure 6 also includes the albedo sensitivity calculated from the time series of spatial variability (dashed lines). There is, not surprisingly, a great range of values, with almost consistently large (negative) values at the months of best correlation. Positive values of sensitivity appear, of course, at the months where the correlation is positive. Region 1 contains more months with extreme negative values (maximum -0.03 K^{-1} for month number 39), and slightly greater albedo sensitivity on average than Region 2. The mean value of $\partial a/\partial$SST in both regions is ≈ -0.01 K^{-1} (slightly larger in Region 1 and slightly smaller in Region 2).

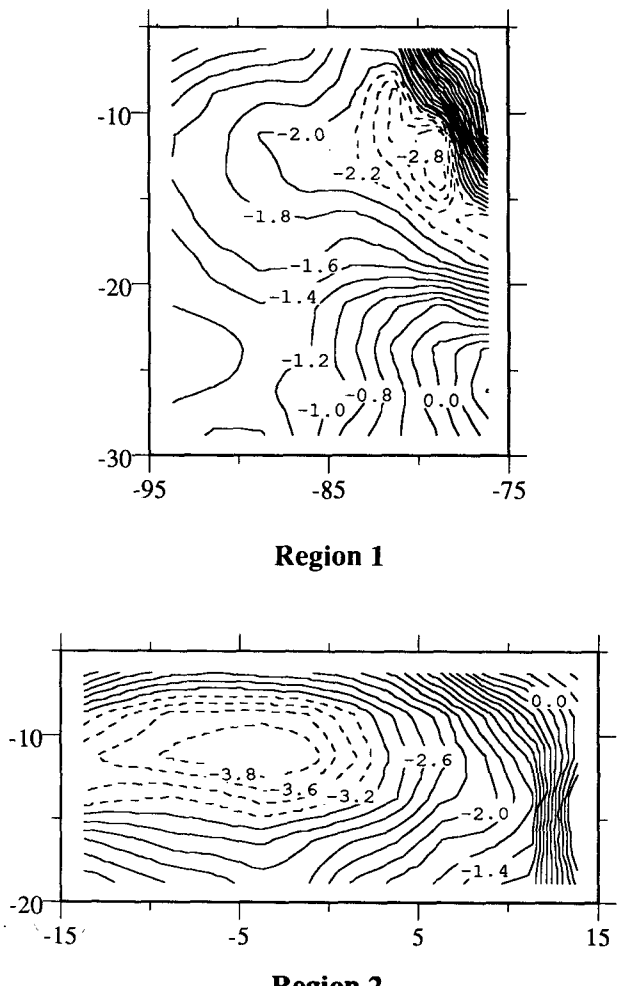

FIG. 10. Fields of the sensitivity term $\partial a/\partial$SST ($\times$ 100). Contour interval is 0.2. The local maxima are highlighted with the dashed contours.

5. Climatic implications

Approximate estimates of mSc feedback have recently been reported by others. Randall et al. (1984) estimated that a 4% (in absolute values) increase in the amount of low oceanic stratus would offset the global warming due to a CO_2 doubling, without, however, explaining how such a conclusion was reached. Hanson (1991) used the 40-yr COADS dataset and a set of assumptions in a series of what he admits to be simplistic computations to estimate that the earth–atmosphere system absorbs an additional 1 W m^{-2} for each 1% decrease in mSc cloud cover. The result, as he pointed out, is in agreement with the Randall et al. (1984) statement (if CO_2 doubling induces a forcing of 4 W m^{-2} at the tropopause). Slingo (1990) used model calculations to find the increase of low-level cloud amount needed to counteract the net radiation changes at the top of the tropopause due to a doubling of CO_2. With the different versions of NCAR Community Climate Model, he obtained increases in cloud cover of 3.5% to 5%—numbers close to those of Randall et al. (1984) and Hanson (1991).

Still, changes in cloud amount are but one way to produce cloud feedback. Changes in cloud microphysics have also received attention, especially in association with marine stratus clouds. Increases in the number of mSc cloud condensation nuclei (CCN) may increase cloud reflectivity for constant liquid water content, due to the increase in cloud droplet number and decrease of cloud droplet radii (Twomey et al. 1984). Coakley et al. (1987) discovered that ship-stack exhausts rich in CCN increase the satellite-observed 0.63-μm and 3.7-μm reflectivities of overlying clouds. Biologically regulated production of CCN may also influence climate according to Charlson et al. (1987), who estimated that a 30% increase in the number of CCN could modify the albedo of low-stratiform water clouds, and increase global albedo by 0.5%. Albrecht (1989) argued that an increase in cloud albedo may be due not only to the direct CCN effect but also to the increased cloud cover resulting from a reduction of drizzle.

The total mSc radiative feedback to climate change cannot be estimated here on the basis of our results. We can, however, estimate the feedback component implied by our results for albedo sensitivity alone for comparison with the above speculations. For this, let us assume that the only cloud radiative feedback is that due to the albedo sensitivity of marine stratocumulus, and consider three scenarios that differ in how this effect is applied globally.

a. Scenario A (global extrapolation by cloud cover)

Here we take an average albedo sensitivity, $\partial a/\partial \mathrm{SST} \approx -0.018\ \mathrm{K}^{-1}$, from the spatial average over our two tropical regions, and assume that this is characteristic of all oceanic stratus. Since the nonoverlapped portion of boundary-layer stratiform clouds covers $\approx$18% of the globe (Charlson et al. 1987) this scenario would lower the earth's albedo by $\approx$0.0032 for a 1-K rise in surface temperature. This corresponds to an increased absorption of $\approx$1.1 W m^{-2} by the system, and positive feedback.

b. Scenario B (global extrapolation by relative cloud forcing)

Here we apply albedo sensitivity globally, based on the observed cloud forcing in the tropics. From ERBE data we find that the annually averaged net cloud forcing in the latitude zone 30°N–30°S is -12.9 W m^{-2}. This number was obtained by taking the mean of the 5-yr average of the four seasons and then averaging over the 3456 grid points without area weighting—a simplification that does not affect the results at low latitudes. If there were no mSc (or other clouds) off the west coasts of Peru, Angola, *and* California (bounded by 15°–30°N and 115°–140°W) so that cloud forcing for these regions was zero, the average net cloud forcing in the tropics would be only -10.6 W m^{-2}. That is, these regions of mSc, which occupy about 6% of the tropics by area, contribute about -2.3 W m^{-2} or 18% of the total tropical cloud forcing. This percentage contribution changes very little when the mSc off the west coasts of Australia and Morocco are added to the calculation.

The global net cloud forcing of -17.3 W m^{-2} (Harrison et al. 1990) is made up of -6.5 W m^{-2} from the tropical half of the planet and -10.8 W m^{-2} from the extratropical half. In this scenario we make the conservative assumption [for higher estimates see Hartmann et al. (1992)] that the relative contribution of mSc to the net forcing in the extratropics is the same as that in the tropics. That is, they contribute 18% of the global net forcing, or about -3 W m^{-2}.

The net cloud forcing averaged over Regions 1 and 2 is ≈ -40 W m^{-2} (also true for the California region). This is about half the peak net forcing observed in the vicinities of local mSc albedo maximum. In this scenario the -40 W m^{-2} value is taken to represent the average net cloud forcing of all mSc. This assumption was based on the subjective interpretation of the results shown by Harrison et al. (1990), Ardanuy et al. (1991), and Klein and Hartmann (1993), and can be explained by taking into account the compensating effects of lower incident insolation and higher solar zenith angles at higher latitudes.

Extrapolating the local average albedo sensitivity of mSc globally scaled by the global to local net cloud forcing contributions of mSc yields a reduction in global albedo of 0.0014 for a 1-K rise in SST. This corresponds to an increased absorption of by the system of $\approx$0.5 W m^{-2}.

c. Scenario C (local effects only)

Here we assume the effects are purely local to Regions 1 and 2, with no global extrapolation. These re-

gions contribute -1.6 W m^{-2} to the tropical net forcing, and -0.8 W m^{-2} to the global average. Since the average cloud radiative forcing in these regions is ≈ -40 W m^{-2}, the global influence is only about 2% of the local effect, similar to the fraction of the earth taken up by these regions.

Taking the local albedo sensitivity as a function of position for the two regions, and weighting by the annual insolation for each position, we found that a 1-K rise in SST would reduce the average cloud forcing for these regions from -40 W m^{-2} to -33 W m^{-2}. This corresponds to an increased absorption by the system of ≈ 0.14 W m^{-2} K^{-1}.

The above scenarios can be directly modified to account for the range of albedo sensitivities found in section 4. At the conservative end of the scale, with an albedo sensitivity of -0.01 K^{-1} half the average, and applying scenario C, the mSc feedback to a 1-K rise is an additional 0.08 W m^{-2}. At the high end of the range, taking an albedo sensitivity of -0.03 K^{-1} and adopting scenario A, the additional absorption becomes 2 W m^{-2} K^{-1}.

6. Summary and discussion

The analysis of five years of ERBE albedo, ISCCP cloud cover, and CAC SST clearly demonstrates that the albedo and total cloud cover of two tropical regions dominated by marine stratocumulus are negatively correlated with sea surface temperature. The correlations generally remain negative irrespective of whether the annual variability, the interannual variability, or the spatial variability for a given month of the data is considered.

Albedo and SST are shown to have clear seasonal cycles that are out of phase. Maximum SST and minimum albedo occurs in February or March, with the reverse occurring in September. Based on annual variability, the correlation coefficients are ≈ -0.8 between both SST and albedo and between SST and total cloud cover. Spatially averaged values indicate a decrease of 0.013 in albedo and 3% in cloud cover for a 1-K rise in temperature for Region 1. The corresponding values are 0.022 and 6% for Region 2. For individual grid points, these values can be as high as 0.03 for albedo and 4.5% for TCC in Region 1, and 0.04 for albedo and 11% for cloud cover in Region 2.

On an interannual basis, colder than average grid elements have statistically higher than average albedo and cloud cover, and vice versa. While the correlation remains negative for interannual variation, quantitative estimates of this and the related albedo sensitivities are influenced by the choice of thresholds needed to exclude background noise. Representative albedo sensitivities are ≈ -0.05 K^{-1} based on the data showing the largest interannual variation (about 3% of the total data).

On a month by month basis, for about 90% of the months, grid points that are colder than the regional average tend to have higher than average albedo/cloud cover, and vice versa. This is true for both regions when considering albedo, but only for Region 2 when considering cloud amount. The degree of correlation varies greatly in a nonsystematic way, however. The average correlation coefficient is ≈ -0.4 for SST–albedo, less negative for SST–TCC. The albedo sensitivity calculated this way averages about -0.01 K^{-1} in both regions but can be as high as -0.03 K^{-1} in specific months.

The above results are consistent with the SST–cloud cover relationships reported by Hanson (1991), Peterson et al. (1992), and Klein and Hartmann (1993) for subtropical and tropical mSc regions, but indicate an additional negative correlation between cloud albedo and SST, beyond the dependence of albedo on cloud cover.

For each region, ranges of temperature can be found where the correlation preserves its negative sign. The correlations deteriorate, or even become positive, above $\approx$25°C or 27°C and below $\approx$19°C or 22°C depending on the region. The grid points that display temperature extremes are usually those close to the boundaries of the selected regions where we would expect to find less mSc. Zonal correlations suggest that there is also a seasonal change in the correlations consistent with the seasonal SST change.

If the statistical relationship between albedo and sea surface temperature reflects an underlying physical relationship, this implies that marine stratocumulus provide an element of positive feedback in the event of climate change. The additional absorption of solar radiation by the earth's climate system in response to a 1-K rise in sea surface temperature ranges from ≈ 0.14 W m^{-2} if the physical mechanism is local to the two regions studied, up to ≈ 1 W m^{-2} if extrapolated to all marine stratocumulus. These values have uncertainties of about $\pm$50% based on the range of albedo sensitivities we have analyzed.

It also seems probable that the potential positive feedback exhibited by mSc is self-bounded in either cooling or warming scenarios because of the change of coupling behavior with SST. Increases in SST possibly lead to a transition to a different cloud regime where the direction of the feedback may be uncertain.

Regions 1 and 2 have many similar characteristics, but also some differences in the way SST and albedo/TCC are correlated. Unlike Region 2, Region 1 has no definite 0-lag correlation maximum. The fields of cross correlation for Region 1 have a greater degree of internal inhomogeneity than for Region 2 and a tendency to display maxima close to the coast if annual variability is under consideration. Region 1 exhibits much stronger interannual albedo and somewhat stronger TCC variability than Region 2. It is possible that this is a consequence of the 1986–87 El Niño. The time series of SST–TCC spatial correlation is dissimilar to that of SST–albedo for Region 1, whereas it is quite similar for Region 2. This may imply that the ISCCP

algorithm encounters difficulties in the retrieval of correct cloud amounts in Region 1 because of the different nature of clouds compared to Region 2 (lower cloud tops, spatially variable degree of breakup).

It is beyond the scope of the present study to provide a complete explanation of the observed response of mSc to sea surface temperature. This behavior has, however, been reproduced in some modeling studies (Wang 1993). The results presented by Klein and Hartmann 1993) and some preliminary analysis of ours for the period December 1986–November 1988 also show a positive correlation between stability and albedo/TCC. This suggests that SST directly affects stability. But as Klein and Hartmann point out there is no obvious reason for why changes in the inversion strength should be associated with cloud amount changes. Evidently, SST or stability do not explain all of the albedo/TCC variance. Other factors such as winds, large-scale divergence, CTEI, cloud–subcloud-layer decoupling, and drizzle have proven to significantly alter cloud fraction and cloud optical properties in model studies (Schubert et al. 1979; Wyant and Bretherton 1992; Wang 1993; Wang et al. 1993) by influencing the profile of buoyancy fluxes, the depth of the boundary layer, and the susceptibility of the cloud deck to breakup.

Finally, the statistical relationships presented here for the present climate must be reproduced and perhaps explained by global climate models before these models can be used successfully to study the effect of cloud radiative feedback. Consequently, these results should serve as a useful diagnostic tool in improving the performance of such models.

Acknowledgments. Partial support for this research by NASA Grant NAGW-1466, the National Science and Engineering Research Council, and the Atmospheric Environment Service is gratefully acknowledged. We would also like to thank Lisa Ramsaran for her technical assistance and two anonymous reviewers for their helpful suggestions.

REFERENCES

Albrecht, B. A., 1989: Aerosols, cloud microphysics, and fractional cloudiness. *Science,* **245,** 1227–1230.

——, 1991: Fractional cloudiness and cloud-top entrainment instability. *J. Atmos. Sci.,* **48,** 1519–1525.

——, D. A. Randall, and S. Nicholls, 1988: Observations of marine stratocumulus clouds during FIRE. *Bull. Amer. Meteor. Soc.,* **69,** 618–626.

——, C. W. Fairall, D. W. Thomson, A. B. White, J. B. Snider, and W. H. Schubert, 1990: Surface based remote sensing of the observed and the adiabatic liquid water content of stratocumulus clouds. *Geophys. Res. Lett.,* **17,** 89–92.

Ardanuy, P. E., L. L. Stowe, A. Gruber, and M. Weiss, 1991: Shortwave, longwave, and net cloud-radiative forcing as determined from *Nimbus 7* observations. *J. Geophys. Res.,* **96,** 18 537–18 549.

Barkstrom, B., E. Harrison, G. Smith, R. Green, J. Kibler, R. Cess, and the ERBE Science Team, 1989: Earth Radiation Budget Experiment (ERBE) archival and April 1985 results. *Bull. Amer. Meteor. Soc.,* **70,** 1254–1262.

Betts, A. K., 1990: Diurnal variation of California coastal stratocumulus from two days of boundary layer soundings. *Tellus,* **42A,** 302–304.

Blaskovic, M., R. Davies, and J. B. Snider, 1991: Diurnal variation of marine stratocumulus over San Nicolas island during July 1987. *Mon. Wea. Rev.,* **119,** 1469–1478.

Bottomley, M., C. K. Folland, J. Hsiung, R. E. Newell, and D. E. Parker, 1990: *Global Surface Temperature Atlas "GOSTA."* U. K. Meteorological Office, Bracknell, 20 pp. and 313 plates.

Bougeault, P., 1985: The diurnal cycle of the marine stratocumulus layer: A higher-order model study. *J. Atmos. Sci.,* **42,** 2826–2843.

Cess, R. D., and collaborators, 1990: Intercomparison and interpretation of climate feedback processes in 19 atmospheric general circulation models. *J. Geophys. Res.,* **95,** 16 601–16 616.

Charlson, R. J., J. E. Lovelock, M. O. Andrae, and S. G. Warren, 1987: Oceanic phytoplankton, atmospheric sulphur, cloud albedo, and climate. *Nature,* **326,** 655–661.

Chen, C. and W. R. Cotton, 1983: A one dimensional simulation of the stratocumulus capped mixed layer model. *Bound.-Layer Meteor.,* **25,** 289–321.

Coakley, J. A., Jr., R. L. Bernstein and P. A. Durkee, 1987: Effect of ship-stack effluents on cloud reflectivity. *Science,* **237,** 1020–1022.

Deardorff, J. W., 1980a: Stratocumulus-capped mixed layers derived from a three-dimensional model. *Bound.-Layer Meteor.,* **18,** 495–527.

——, 1980b: Cloud-top entrainment instability. *J. Atmos. Sci.,* **37,** 131–147.

Duynkerke, P. G., and A. G. M. Driedonks, 1987: A model for the turbulent structure of the stratocumulus-topped atmospheric boundary layer. *J. Atmos. Sci.,* **44,** 43–64.

Fairall, C. W., J. E. Hare, and J. B. Snider, 1990: An eight-month sample of marine stratocumulus cloud fraction, albedo, and integrated liquid water. *J. Climate,* **3,** 847–864.

Hanson, H. P., 1991: Marine stratocumulus climatologies. *Int. J. Climatol.,* **11,** 147–164.

Harrison, E. F., P. Minnis, B. R. Barkstrom, V. Ramanathan, R. D. Cess, and G. G. Gibson, 1990: Seasonal variation of cloud radiative forcing derived from the Earth Radiation Budget Experiment. *J. Geophys. Res.,* **95,** 18 687–18 703.

Hartmann, D. L., M. E. Ockert-Bell, and M. L. Michelsen, 1992: The effect of cloud type on the earth's energy balance: Global analysis. *J. Climate,* **5,** 1281–1304.

Kahn, P. H., and J. A. Businger, 1979: The effect of radiative flux divergence on entrainment of a saturated convective boundary layer. *Quart. J. Roy. Meteor. Soc.,* **105,** 303–306.

Klein, S. A., and D. L. Hartmann, 1993: The seasonal cycle of low stratiform clouds. *J. Climate,* **6,** 1587–1606.

Kuo, H., and W. H. Schubert, 1988: Stability of cloud-topped boundary layers. *Quart. J. Roy. Meteor. Soc.,* **114,** 887–917.

Lilly, D. K., 1968: Models of cloud-topped mixed layers under a strong inversion. *Quart. J. Roy. Meteor. Soc.,* **94,** 292–309.

MacVean, M. K., and P. J. Mason, 1990: Cloud-top entrainment instability through small-scale mixing and its parameterization in numerical models. *J. Atmos. Sci.,* **47,** 1012–1030.

McFarlane, N. A., G. J. Boer, J. P. Blanchet, and M. Lazare, 1992: The Canadian Climate Center second generation general circulation model and its equilibrium climate. *J. Climate,* **5,** 1013–1044.

Mitchell, T. P., and J. M. Wallace, 1992: The annual cycle in equatorial convection and sea surface temperature. *J. Climate,* **5,** 1140–1156.

Moeng, C. H., and A. Arakawa, 1980: A numerical study of marine subtropical stratus cloud layer and its stability. *J. Atmos. Sci.,* **37,** 2661–2676.

Newell, R. E., J. W. Kidson, D. G. Vincent, and G. J. Boer with contributions by J. R. Holton, J. M. Wallace, T. G. Dopplick,

and Arthur C. Kyle, 1974: *The General Circulation of the Tropical Atmosphere and Interactions with Extratropical Latitudes, vol. 2.* MIT Press, 371 pp.

Nicholls, S., 1984: The dynamics of stratocumulus: Aircraft observations and comparisons with a mixed layer model. *Quart. J. Roy. Meteor. Soc.*, **110,** 783–820.

Nucciarone, J. J., and G. S. Young, 1991: Aircraft measurements of turbulence spectra in the marine stratocumulus-topped boundary layer. *J. Atmos. Sci.*, **48,** 2382–2392.

Oreopoulos, L., 1992: Tropical marine stratocumulus albedo and its relation to sea surface temperature. MSc. thesis, Dept. of Atmospheric Sciences, McGill University, 805 Sherbrooke St. West, Montreal, Canada, H3A-2K6. 111 pp.

Paluch, I. R., and D. H. Lenschow, 1991: Stratiform cloud formation in the marine boundary layer. *J. Atmos. Sci.*, **48,** 2141–2158.

Peterson, T. C., T. P. Barnett, E. Roeckner, and T. H. Vonder Haar, 1992: An analysis of the relationship between cloud anomalies and sea surface temperature anomalies in a global circulation model. *J. Geophys. Res.*, **97,** 20 497–20 506.

Ramanathan, V., R. D. Cess, E. F. Harrison, P. Minnis, B. R. Barkstrom, E. Ahmad, D. Hartmann, 1989: Cloud-radiative forcing and climate: Results from the Earth Radiation Budget Experiment. *Science,* **243,** 57–63.

Randall, D. A., 1980: Conditional instability of the first kind upside down. *J. Atmos. Sci.*, **37,** 125–130.

——, Coakley, J. A., Fairall, C. W., Kropfli, R. A., and Lenschow, D. H., 1984: Outlook for research on subtropical marine stratiform clouds. *Bull. Amer. Meteor. Soc.*, **65,** 1290–1301.

Reynolds, R. W., 1988: A real-time global sea surface temperature analysis. *J. Climate,* **1,** 75–86.

Riehl, H., 1979: *Climate and Weather in the Tropics.* Academic Press, 611 pp.

Rossow, W. B., and R. A. Schiffer, 1991: ISCCP cloud data products. *Bull. Amer. Meteor. Soc.*, **72,** 2–20.

Schubert, W. H., 1976: Experiments with Lilly's cloud-topped mixed layer model. *J. Atmos. Sci.*, **33,** 436–446.

——, J. S. Wakefield, E. J. Steiner, and S. K. Cox, 1979: Marine stratocumulus convection. Part I: Governing equations and horizontally homogeneous solutions. *J. Atmos. Sci.*, **36,** 1286–1307.

Slingo, A., 1990: Sensitivity of the Earth's radiation budget to changes in low clouds. *Nature,* **343,** 49–51.

Stephens, G. L., and T. J. Greenwald, 1991: The Earth's radiation budget and its relation to atmospheric hydrology. 2. Observations of cloud effects. *J. Geophys. Res.*, **96,** 15 325–15 340.

Tselioudis, G., W. B. Rossow, and D. Rind, 1992: Global patterns of cloud optical thickness variation with temperature. *J. Climate,* **5,** 1484–1495.

Turton, J. D., and S. Nicholls, 1987: A study of the diurnal variation of stratocumulus using a multiple mixed layer model. *Quart. J. Roy. Meteor. Soc.*, **113,** 969–1009.

Twomey, S. A., M. Piepgrass, and T. L. Wolfe, 1984: An assessment of the impact of pollution on global cloud albedo. *Tellus,* **36B,** 356–366.

Wang, S., 1993: Modeling marine boundary layer clouds with a two-layer model: A one-dimensional simulation. *J. Atmos. Sci.*, **50,** 4001–4021.

——, B. A. Albrecht, and P. Minnis, 1993: A regional simulation of marine boundary layer clouds. *J. Atmos. Sci.*, **50,** 4022–4043.

Warren, S. G., C. J. Hahn, J. London, R. M. Chervin, and R. L. Jenne, 1988: *Global Distribution of Total Cloud Cover and Cloud Type Amounts Over Ocean.* NCAR Tech. Note NCAR/TN − 317 + STR, National Center for Atmospheric Research, P.O. Box 3000, Boulder, CO 80307. 42 pp. plus 170 maps.

Wielicki, B. A., and L. Parker, 1992: On the determination of cloud cover from satellite sensors: The effect of sensor spatial resolution. *J. Geophys. Res.*, **97,** 12 799–12 823.

Wyant, M. C., and C. S. Bretherton, 1992: The dynamics of decoupling in a cloud-topped boundary layer. *Proc. 11th ICCP,* Montreal, 417–420.